Draft version January 26, 2002
Preprint typeset using LaTeX style emulateapj v. 14/09/00

THE LAS CAMPANAS IR SURVEY: EARLY TYPE GALAXY PROGENITORS BEYOND REDSHIFT ONE

P. J. McCarthy[1], R. G. Carlberg[2], H.-W. Chen[1], R. O. Marzke[1,3], A. E. Firth[4], R. S. Ellis[5], S. E. Persson[1], R. G. McMahon[4], O. Lahav[4], J. Wilson[1], P. Martini[1], R. G. Abraham[2], C. N. Sabbey[4], A. Oemler[1], D. C. Murphy[1], R. S. Somerville[4] M. G. Beckett[1,4], J. R. Lewis[4], C. D. MacKay[4]

Accepted for publication in the Astrophysical Journal Letters

ABSTRACT

We have identified a population of faint red galaxies from a 0.62 square degree region of the Las Campanas Infrared Survey whose properties are consistent with their being the progenitors of early-type galaxies. The optical and IR colors, number-magnitude relation and angular clustering together indicate modest evolution and increased star formation rates among the early-type field population at redshifts between one and two. The counts of red galaxies with H magnitudes between 17 and 20 rise with a slope that is much steeper than that of the total H sample. The surface density of red galaxies drops from roughly 3000 per square degree at $H = 20.5, I - H > 3$ to ~ 20 per square degree at $H = 20, I - H > 5$. The $V - I$ colors are approximately 1.5 magnitudes bluer on average than a pure old population and span a range of more than three magnitudes. The strength of the angular clustering of the red galaxies is an order of magnitude larger than that of the full galaxy sample. The colors, and photometric redshifts derived from them, indicate that the red galaxies have redshift distributions adequately described by Gaussians with $\sigma_z \simeq 0.2$ centered near redshift one, with the exception that galaxies having $V - I < 1.6$ and $I - H > 3$ are primarily in the $1.5 \lesssim z \lesssim 2$ range. We invert the angular correlation functions using these n(z) and find co-moving correlation lengths of $r_0 \simeq 9 - 10h^{-1}$Mpc at $z \simeq 1$, comparable to, or larger than, those found for early-type galaxies at lower redshifts. A simple photometric evolution model reproduces the counts of the red galaxies, with only a $\sim 30\%$ decline in the underlying space density of early-type galaxies at $z \sim 1.2$. The colors indicate characteristic star formation rates of $\sim 1 M_\odot/yr$ per $10^{10} M_\odot$. We suggest on the basis of the colors, counts, and clustering that these red galaxies are the bulk of the progenitors of present day early-type galaxies.

Subject headings: surveys — — — galaxies: evolution — — — galaxies: high redshift

1. INTRODUCTION

The earliest deep images at high latitude obtained with near-IR arrays revealed a population of galaxies not represented in optical surveys (e.g. Elston, Rieke, & Rieke 1988; McCarthy, Persson & West 1992; Hu & Ridgway 1994). These objects have colors and apparent magnitudes close to those expected of evolved massive galaxies at $1 < z < 3$. Selections based on $R - K$ lead to a heterogeneous population containing evolved stellar populations (Spinrad et al. 1997; Soifer et al. 1999), reddened objects (Graham & Dey 1996; Cimatti et al. 1998; Dey et al. 1999, Barger et al. 2000), and cool stars. Redshifts for either dust-free or highly reddened objects are primarily in the $1 < z < 2$ range (Graham & Dey 1996; Soifer et al. 1999; Liu et al. 2000, Cowie et al. 2001). While the reddest examples (Smail et al 1999) are sometimes associated with bright sub-mm sources and cm-wave sources, the bulk of the red galaxies do not appear to be strong cm to sub-mm continuum sources.

A key issue in the hierarchical assembly picture of galaxy formation is the identification of the redshift range over which the most massive galaxies assemble. The effects of merging at $z < 1$ are minor: the luminosity function evolves primarily through passive evolution (Lilly et al. 1995, Cowie et al. 1996) and the merger rate is low (Carlberg et al 2000). The rate of mass buildup via merging is dependent on the density of galaxies, the correlation function at relevant separations, and the distribution of pairwise velocities. For major mergers to play a dominant role in galaxy building, the clustering of at least some component of the normal galaxy population must be large relative to that at the current epoch. Near-IR selection provides a powerful tool for removing the foreground of faint low redshift star forming galaxies and offers a path toward selecting galaxies at $z \sim 1$ by stellar mass.

The Las Campanas Infrared (LCIR) survey was crafted to select early-type galaxies at $1 < z < 2$ (Marzke et al. 1999). It is a near-IR survey to $H \sim 21$ over a significant fraction of a square degree, supplemented by photometry in the UBVRIz′ bands. In this *Letter* we present the basic observational results for the galaxy counts, colors and clustering properties, along with their implications based on simple modeling. Future papers will augment these data and refine and broaden the interpretation.

[1] Carnegie Observatories, 813 Santa Barbara St, Pasadena, CA 91101
[2] Department of Astronomy, University of Toronto, Toronto ON, M5S 3H8 Canada
[3] Department of Astronomy and Physics, San Francisco State University, San Francisco, CA
[4] Institute of Astronomy, Cambridge CB3 OHA, UK
[5] Department of Astronomy, Caltech 105-24, Pasadena, CA 91125

2. OBSERVATIONS & RESULTS

2.1. *Observations*

The data presented here are drawn from a subset of the LCIR survey covering an area of 0.62 square degrees to a depth ranging from H= 20 to 21 in four fields: Hubble Deep Field South (HDFS), Chandra Deep Field South (CDFS), SSA22 and the NTT Deep Field. The H data, obtained with the CIRSI camera (Beckett et al. 1998), are complemented by deep optical imaging: VRI in all fields, U & B in HDFS, and z′ in CDFS. The details of the near-IR survey are described in Chen et al. (2001*a*) and Firth et al. (2001), while the optical data are discussed in Marzke et al. (in prep). Photometric catalogs were extracted for each field using 4″ aperture Johnson magnitudes.

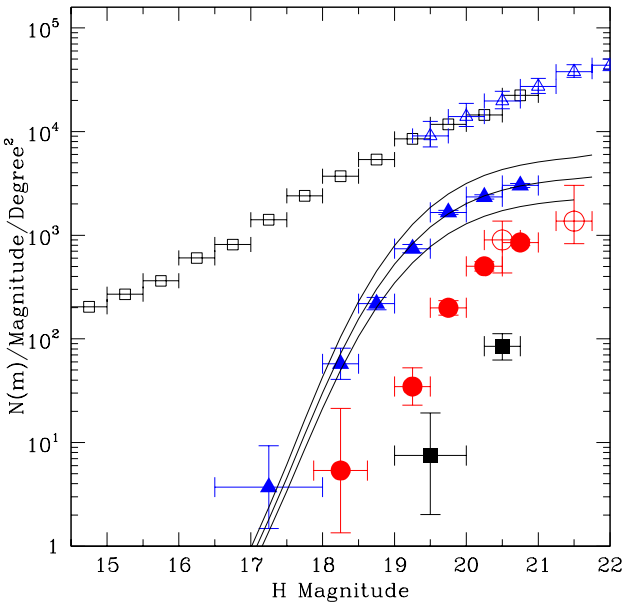

FIG. 1.— The total and red galaxy counts as a function of H magnitude over 0.62 square degrees in four fields. The open squares represent the complete galaxy sample, after removal of stars. The open triangles are the NICMOS based H counts from Yan et al. (1997). The filled triangles and circles are the H counts for $I-H>3$ and 4, respectively. The error bars show the 95% confidence interval assuming Poisson statistics. The open circles at $H=20.5$ and 21.5 are from the $R-H>5$ NICMOS sample of Yan et al. (2000). The filled squares are the counts for $I-H>5$ from the CDFS and HDFS fields only. The curves show the counts for $I-H>3$ derived from the evolving population models described in the text with $p=0, 0.5$, and 1. The characteristic redshift for the $I-H>3$ model is 1.2.

2.2. *N(m) for Red Galaxies*

In Figure 1 we present the differential number magnitude relations for the complete H selected sample and $I-H$ color selected sub-samples from the HDFS, CDFS, SSA22 and NTT fields. These counts are based on 4″ aperture magnitudes with aperture and incompleteness corrections derived from point sources. Each field was used only to its 95% completeness limit. A full analysis of the number counts and their completeness are given in Chen et al. (2001*a*) and Firth et al. (2001). The complete H counts are similar in slope, dlog(n)/dm, and amplitude to the deep H counts derived by Yan et al. (1997). The $I-H>3$ counts are quite steep, dlog(n)/dm= 1.1 in the $17<$ H <19.5 range. At fainter levels the counts must flatten and the slope of the $I-H>3$ subsample appears to change near $H=19.5$. The counts in the redder color bin appear to have the same slope as the $I-H>3$ counts for $H<20$ but with surface densities that fall roughly one order of magnitude per magnitude of increasingly red color. At bright magnitudes (e.g. H$\sim$ 17.5) the red galaxies constitute roughly 0.5% of the total H selected population with a surface density of a few per square degree, while at H= 20.5 they contribute roughly 10% of the total population at a density of ~ 3000 per square degree. We note that our primary color-cut, $I-H>3$, is roughly one magnitude bluer than the canonical "ERO" color threshold of $R-K>6$.

We use a set of simple evolutionary models to examine both the red counts and the colors (§ 2.3), computed with the PEGASE.2 code (Fioc & Rocca-Volmerange 1997) and the Gardner et al. (1997) local K-band luminosity function. We identify the red galaxy population as those galaxies brighter than M_*-1 as fitted with a Schechter function with $\alpha=1$ and $M_*(\mathrm{red})=M_*-0.2$ and $\phi_*(\mathrm{red})=0.15\phi_*$. Assuming the $I-H$ colors at the faint limit of our sample have a precision of 0.25 magnitudes, this model luminosity function is evolved using a $\tau=1$ decaying star formation rate model and a number density that evolves as $(1+z)^{-p}$ in a $\Omega_M=0.3, \Omega_\Lambda=0.7$ cosmology to predict the red galaxy number counts in Figure 1. Density evolution with $p=0.5\pm0.2$ agrees well with the observed counts of galaxies with $I-H>3$, and implies a decline in true space density of $\sim 30\%$ at $z=1.2$.

There have been a variety of measurements of the surface density of red objects from near-IR surveys, primarily based on R - K selected samples. At the faint end our surface density of 1000 per square degree for $I-H>4$ agrees well with the NICMOS measurements reported by Yan et al. (2000) for $R-H>5$. Our counts at $H=20, I-H>4$ agree well with the surface density of 150 per square degree for $R-K>6, K<19.0$ reported by Thompson et al. (1999) and our counts at $I-H>3$ agree with those reported by Daddi et al. (2000) for $R-K>5$.

2.3. *Optical and Near-IR Colors*

Stars and galaxies at different redshifts have distinctive signatures in an optical near-IR color-color diagram. In Figure 2 we plot the $V-I$ vs. $I-H$ diagram from the CDFS field, for $19\leq H\leq 20.5$. The points are color-coded on the basis of photometric redshifts (Chen et al. 2001*b*; Firth et al. 2001). The red galaxies with $I-H>3$ span more than three magnitudes in $V-I$. This wide range of optical colors worked against previous searches for early-type galaxies at $z>1$ that required colors that matched purely passive models. It is particularly notable that very few of the red galaxies have $V-I\sim 3$, the color expected of purely old stellar populations. Our estimated 50% completeness limit in V is slightly beyond 26 magnitudes, so we should be missing very few of these inactive red galaxies. Few such objects are seen in deeper fields (e.g. Moustakas et al. 1997) We note that our survey area is such that we only sample the field population and expect to detect few, if any, rich clusters.

Superimposed on the data in Figure 2 are the loci of four evolutionary models spanning the $0<z<2$ range computed using the PEGASE.2 code (Fioc & Rocca-

Volmerange 1997). Note that virtually all objects to the left of the models are stars. With increasing redshift the colors initially become redder, but as the V band begins to sample the rest UV part of the spectrum beyond $z = 1$ it begins to brighten. The model that best matches the red galaxy population, an exponentially declining star formation rate with $\tau = 1$Gy, is the same model that reproduces the red counts shown in Figure 1. At the redshift of observation the star-formation rates are not insignificant, the rate being $\sim 1 M_\odot/yr$ per $10^{10} M_\odot$, comparable to the star formation rates in the general field galaxy population at comparable redshifts. The $I-H$ defined red galaxies with the bluest $V-I$ colors are expected to lie at $1.5 < z < 2$ on the basis of this model. The photometric redshifts support this as shown by the significant number of $z_{ph} > 1.5$ objects in the lower right portion of the color-color plane.

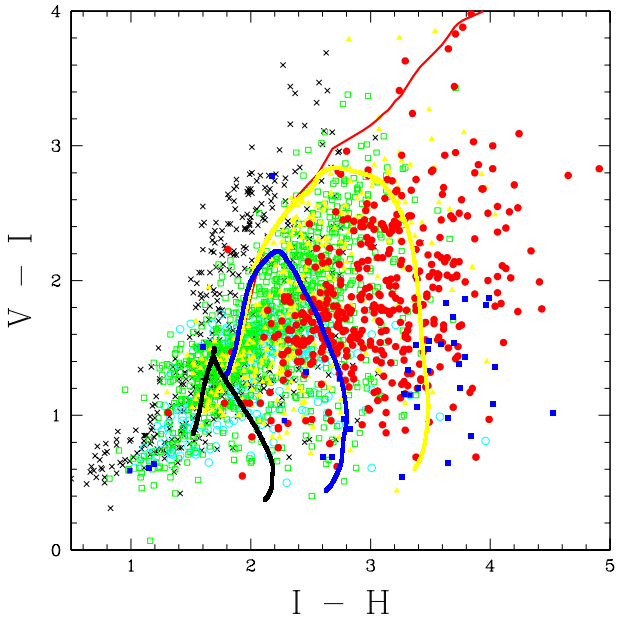

FIG. 2.— The $V-I$ vs. $I-H$ colors for objects with $19 < H < 20.5$ in the CDFS field. The points are color coded on the basis of their photometric redshift: stars (black, crosses), $z < 0.25$ (cyan, open circles), $0.25 < z < 0.75$ (green, open squares), $0.75 < z < 1.0$ (yellow, filled triangles), $1 < z < 1.5$ (red, filled circles), and $1.5 < z < 2.0$ (blue, filled squares). The model curves show the loci of evolving population models with various star formation laws: a single burst with $z_f = 30$ (red), exponentially decline with $\tau = 1\&2$ Gyr (yellow and blue), and continuous (black). The yellow curve is from the same model used in Figure 1.

2.4. *Angular Clustering*

We have computed the angular correlation function of the red objects in our fields. The deepest and most complete data sets come from the HDFS and CDFS survey areas. The CDFS field covers 561 $\Box'$ with an average 90% completeness H depth of 20.5, The HDFS field covers 847 $\Box'$ to an average 90% completeness depth of 20.1. We use the Landy & Szalay (1993) algorithm for estimating $\omega(\theta)$. Uncertainties are computed from the differences between the two fields. We use the population of stars and faint blue galaxies as the random distribution. As a check we determined $\omega(\theta)$ for a complete H-selected sample using a generated random sample and a completeness map for a sub-region of the HDFS field and recover a clustering angle of approximately $2''$.

In Figure 3 we display the angular correlation function for the full H-selected population and for the red galaxies in three apparent magnitude bins, $18 < H < 19$, $19 < H < 20$, and $20 < H < 20.5$. The correlation angles, θ_0, derived from fits to $\omega(\theta) = (\theta_0/\theta)^{\gamma-1}$ ($\gamma = 1.8$ is assumed), are given in Table 1. The clustering shows very steep color and magnitude dependencies, allowing a strong test of the estimated redshift distribution and the spatial correlation length. There are two primary trends: the red galaxies are very much more correlated than the entire H limited sample, and, the angular clustering increases much faster with decreasing limiting magnitude than can be expected on the basis of depth in a uniformly distributed population. The natural interpretation is that the red galaxies are distributed in a relatively narrow redshift shell around $z = 1$. In Table 1 we report the dependence of clustering on color in various sub-samples and find that the clustering increases for progressively redder subsamples. We split the $I-H > 3$ galaxies into sub-samples with red and blue rest-frame UV colors at $V-I = 1.8$, finding that both sub-samples have increased correlations compared to the whole, and hence occupy narrower redshift ranges.

2.5. *Spatial Clustering*

The red galaxy counts, colors, and angular clustering together allow us to infer their statistical distribution in redshift. Here we present a simple population model approach using the evolving luminosity function as described in § 2.2.

To invert the θ_0 into co-moving correlation length, $r_0(z)$, we use the relativistic generalization of Limber's equation for $\xi(r,z) = (r_0(z)/r)^\gamma$,

$$\omega(\theta) = A(\gamma)\theta^{1-\gamma} N^{-2} \int n^2(z) r_0^\gamma(z) x^{1-\gamma} \frac{H(z)}{c} dz, \quad (1)$$

where $N = \int n(z)\,dz$, $A(\gamma) = \Gamma(\frac{1}{2})\Gamma((\gamma-1)/2)/\Gamma(\gamma/2)$, and $H(z) = H_0[\Omega_M(1+z)^3 + \Omega_R(1+z)^2 + \Omega_\Lambda]^{1/2}$, with $\Omega_M + \Omega_R + \Omega_\Lambda = 1$. The co-moving distance, $x(z)$, is computed for our adopted cosmology $\Omega_M = 0.3, \Omega_\Lambda = 0.7$.

We approximate the $n(z)$ distributions with Gaussians fit to the results of the population model discussed in § 2.2 (see Table 1). Determinations of $n(z)$ from our photometric redshifts in the CDFS field yield mean redshifts and characteristic widths for the $I-H > 3$ and $I-H > 3.5$ sub-samples quite close to those listed in Table 1. An additional constraint comes from redshifts for objects in similar color and magnitude ranges from the Caltech Faint Galaxy Redshift Survey (Cohen et al. 1999). The Cohen et al. sample is K selected, but if we adopt $H-K = 1$ for the red population, we can compare the redshift distribution of their $K = 20$ sample. A red color cut yields $< z >= 1.2$, $\sigma_z \sim 0.15$, a distribution somewhat narrower than that derived from the photometric redshifts, as expected. We use our population model to mitigate the small number statistics in the photometric redshifts, particularly for the reddest colors and brightest magnitudes. We adopt $< z >= 1.2$ for the red galaxies, 0.9 for the $18 \le H \le 19$ range and 1.6 for the $V-I < 1.8$ blue sub-sample of the $I-H$ red galaxies.

The inferred co-moving correlation lengths, r_o, are listed in Table 1. The correlation lengths increase as $\sigma_z^{0.55}$ and

have only a very weak dependence on the mean redshift. Although these correlation lengths are large, they are comparable to those found for early-type galaxy populations at low redshifts (Davis & Geller 1976, Guzzo et al. 1997, Willmer, da Costa & Pellegrini 1998). Our larger inferred values of r_0 at high redshift compared to local early-types could be the result of an increasing biasing with redshift, as expected theoretically (Mo & White 1996), or simply an overestimate of the width of the redshift distribution.

3. CONCLUSIONS

We have identified a large sample of faint red galaxies from a 0.62 square degree area of the Las Campanas IR Survey. While the present data set does not allow a direct constraint on the contribution from heavily reddening star forming galaxies, the counts, colors and clustering statistics of these galaxies are all consistent with their being a mildly evolved progenitor of the present day early-type field population. We find evidence for a modest change in the co-moving space density of early-type galaxies to $z \sim 1.2$. The star formation rates inferred from the rest-frame UV colors suggests that the objects are largely, but not completely, assembled by the epoch of observation. If the red galaxies are predominantly old stellar systems, their numbers are larger than predicted in galaxy evolution models with strong merging (e. g. Kauffmann & Charlot 1998, Somerville et al 2001). The use of a color selection that does not extend to the rest-frame UV allows us to recognize nearly-passively evolving objects with greater confidence than selections spanning large color baselines.

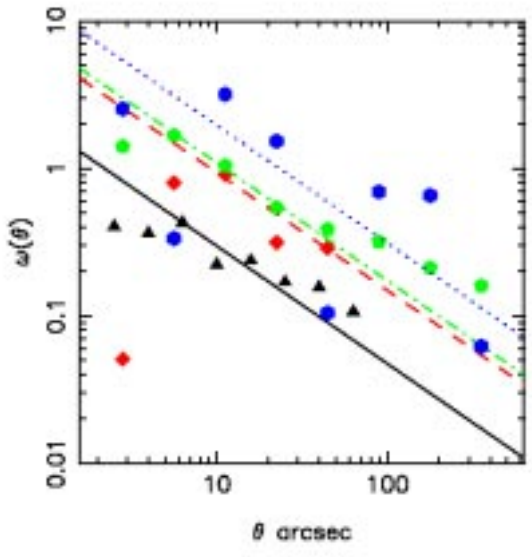

FIG. 3.— The angular correlation function for various color and magnitude sub-samples: all colors for $19 < H < 20.5$ (black triangles), and $I - H > 3$ samples with $18 \leq H \leq 19$(blue circles), $19 \leq H \leq 20$ (green pentagons), and $20 \leq H \leq 20.5$ (red diamonds). The strong increase with increasing brightness is primarily the result of a narrowing redshift distribution. In all cases $r_0 \sim 9h^{-1}$ Mpc.

4. ACKNOWLEDGMENTS

This research was supported by the National Science Foundation under grant AST-9900806 and NSERC of Canada. The CIRSI camera was made possible by the generous support of the Raymond and Beverly Sackler Foundation.

REFERENCES

Barger, A.J., Cowie, L.L. & Richards, E.A. 2000, AJ, 119, 2092
Beckett, M. G., MacKay, C. D., McMahon, R. G., Parry, I. R., Ellis, R. S., Chan, S. J., Hoenig, M. 1998, SPIE, 3354, 431
Carlberg, R. G., Cohen, J., Patton, D., Blandford, R., Hogg, D., Yee, H., Morris, S. et al. 2000, ApJ, 532, 1
Chen H.-W., McCarthy, P., Marzke, R., Wilson, J., Carlberg, R., Firth, A. Persson, S., Sabbey, C., et al. 2001*a*, ApJ, submitted
Chen H.-W., McCarthy, P., Marzke, R., Wilson, J., Carlberg, R., Firth, A. Persson, S., Sabbey, C., et al. 2001*b*, in prep.
Cimatti, A., Andreani, P., Rottgering, H., Tilanus, R. 1998, Nature, 392, 895
Cohen, J. G., Hogg, D. W., Blandford, R., Cowie, L. L., Hu, E., Songaila, A., Shopbell, P. & Richberg, K. 1999, ApJ, submitted
Cowie, L. L., Songaila, A., Hu, E. M., & Cohen, J. G. 1996, AJ, 112, 839
Cowie, L. L, Barger, A. J., Bautz, M. W., Capak, P. Crawford, C. S., Fabian, A. C., Hu, E., Iwamuro, F., Kneib, J., Maihara, T., Motohara, K. 2001, ApJ, 551, 9
Daddi, E., Cimatti, A., Pozzetti, L., Hoekstra, H., Rottgering, H., Renzini, A., Zamorani, G., Manucci, F. 2000, A&A, 361, 535
Davis, M. & Geller, M. J, 1976, ApJ 203, 13
Dey, A. , Graham, J. R., Ivison, R. J., Smail, I. , Wright, G. S. & Liu, M. C. 1999, ApJ, 519, 610
Elston, R., Rieke, G. H. & Rieke, M. J. 1988, ApJ, 331, L77
Firth, A. E., Somerville, R., Lahav. O., McMahon, R., Sabbey, C., Ellis, R., McCarthy, P. et al. 2001, MNRAS, submitted
Gardner, J., Sharples, R. M., Frenk, C. S., Carrasco, B. E. 1997, ApJ, 480, L99
Graham, J. R. & Dey, A. 1996, ApJ, 471, 720
Guzzo, L., Strauss, M. A., Fisher, K. B., Giovanelli, R. & Haynes, M. P. 1 997, ApJ, 489, 37
Hu, E. M. & Ridgway, S. E. 1994, AJ, 107, 1303
Fioc, M. & Rocca-Volmerange, B. 1997, A&A, 326, 950
Kauffmann, G. & Charlot, S. 1998, MNRAS, 297, L23
Landy, S. D. & Szalay, A. S. 1993, ApJ, 412, 64
Lilly, S. J., Tresse, L., Hammer, F., Crampton, D., Le Fevre, O. 1995, ApJ, 455, 108
Liu, M. C., Dey, A., Graham, J., Bundy, K., Steidel, C., Adelberger, K., Dickinson, M. 2001, AJ, 119, 2556
Marzke, R. O., McCarthy, P., Persson, E., Oemler, A., Dressler, A., Yan, M. Beckett, M., Carlberg, R. et al. 1999, in Photometric Redshifts and the Detection of High Redshift Galaxies, ASP conf. series 191, p. 148, eds. R. Weymann, L. Storrie-Lombardi, M. Sawicki, & R. Brunner.
McCarthy, P. J., Persson, S. E. & West, S. C. 1992, ApJ, 386, 52
Mo, H. J. & White, S. D. M. 1996, MNRAS, 282, 347
Moustakas, L., Davis, M., Graham, J., Peterson, B., Silk, J. 1997, AJ, 475, 445
Smail, I., Ivison, R., J., Kneib, J.-P., Barger, A., Owen, F., Morisson, G. 1999, MNRAS, 308, 1061
Soifer, B. T., Matthews, K., Neugebauer, G., Armus, L., Cohen, J. G., Persson, S. E., Smail, I. 1999, AJ, 118, 2065
Somerville, R. S., Primack, J. R., & Faber, S. M. 2001, MNRAS, 320, 504
Spinrad, H., Dey, A., Stern, D., Dunlop, J., Peacock, J., Jimenez, R., WIndhorst, R. 1997, ApJ, 484, 581
Thompson, D., Beckwith, S., Fockenbrock, R., Fried, J., Hippelein, H., Huang, J., van Kuhlmann, B., Leinert, Ch. et al. 1999, ApJ, 523, 100
Willmer, C. N. A., da Costa, L. N. & Pellegrini, P. S. 1998, AJ, 115, 869
Yan, L., McCarthy, P., Weymann, R., Malkan, M., Teplitz, H., Storrie-Lombardi, L., Smith, M., Dressler, A. 2000, AJ, 120, 575
Yan, L., McCarthy, P., Storrie-Lombardi, L., Weymann, R. J. 1998, ApJ, 503, 19

Table 1. Clustering Properties of Red Galaxies

Subsample		θ_0			r_0
H	$I-H$	($''$)	$< z >$	σ_z	h^{-1}Mpc
$20.0-20.5$	$3.0-5.0$	5.0 ± 0.2	1.2	0.30	8.4
$19.0-20.0$	$3.0-5.0$	15.0 ± 1.0	1.2	0.15	9.5
$18.0-19.0$	$3.0-5.0$	50.0 ± 7.0	0.9	0.07	10.7
$20.0-20.5$	ALL	2.0 ± 0.2	0.7	0.30	5.7
$19.0-20.5$	$3.0-5.0$	6.7 ± 0.4	1.2	0.30	9.8
$19.0-20.5$	$3.5-5.0$	6.3 ± 0.5	1.2	0.30	9.5
$19.0-20.5$	$4.0-5.0$	11 ± 0.5	1.2	0.20	9.7
$19.0-20.5^{\dagger}$	$3.0-5.0$	15 ± 2	1.2	0.15	9.6
$19.0-20.5^{\dagger\dagger}$	$3.0-5.0$	12 ± 1	1.6	0.2	9.8

$\dagger V-I > 1.8$, $\dagger\dagger V-I < 1.8$.